Aerosol and Air Quality Research, 16: 2802–2817, 2016

ISSN: 1680-8584 print / 2071-1409 online
doi: 10.4209/aaqr.2016.03.0130

Radiative Effect of Springtime Biomass-Burning Aerosols over Northern Indochina during 7-SEAS/BASELInE 2013 Campaign

Shantanu Kumar Pani[1], Sheng-Hsiang Wang[1*], Neng-Huei Lin[1,2*], Chung-Te Lee[3], Si-Chee Tsay[4], Brent N. Holben[4], Serm Janjai[5], Ta-Chih Hsiao[3], Ming-Tung Chuang[3], Somporn Chantara[2]

[1] *Department of Atmospheric Sciences, National Central University, Chung-Li 32001, Taiwan*
[2] *Environmental Science Program, Faculty of Science, Chiang Mai University, Chiang Mai, Thailand*
[3] *Graduate Institute of Environmental Engineering, National Central University, Chung-Li 32001, Taiwan*
[4] *Goddard Space Flight Center, NASA, Greenbelt, Maryland, USA*
[5] *Department of Physics, Faculty of Science, Silpakorn University, Nakhon Pathom, Thailand*

ABSTRACT

The direct aerosol radiative effects of biomass-burning (BB) aerosols over northern Indochina were estimated by using aerosol properties (physical, chemical, and optical) along with the vertical profile measurements from ground-based measurements with integration of an optical and a radiative transfer model during the Seven South East Asian Studies/ Biomass-Burning Aerosols & Stratocumulus Environment: Lifecycles & Interactions Experiment (7-SEAS/BASELInE) conducted in spring 2013. Cluster analysis of backward trajectories showed the air masses arriving at mountainous background site (Doi Ang Khang; 19.93°N, 99.05°E, 1536 m above mean sea level) in northern Indochina, mainly from near-source inland BB activities and being confined in the planetary boundary layer. The PM_{10} and black carbon (BC) mass were 87 ± 28 and 7 ± 2 μg m^{-3}, respectively. The aerosol optical depth (AOD_{500}) was found to be 0.26–1.13 (0.71 ± 0.24). Finer (fine mode fraction ≈0.95, angstrom-exponent at 440–870 nm ≈1.77) and significantly absorbing aerosols (single-scattering albedo ≈0.89, asymmetry-parameter ≈0.67, and absorption AOD ≈0.1 at 440 nm) dominated over this region. BB aerosols (water soluble and BC) were the main contributor to the aerosol radiative forcing (ARF), while others (water insoluble, sea salt and mineral dust) were negligible mainly due to their low extinction efficiency. BC contributed only 6% to the surface aerosol mass but its contribution to AOD was 12% (2 times higher). The overall mean ARF was –8.0 and –31.4 W m^{-2} at top-of-atmosphere (TOA) and at the surface (SFC), respectively. Likely, ARF due to BC was +10.7 and –18.1 W m^{-2} at TOA and SFC, respectively. BC imposed the heating rate of +1.4 K d^{-1} within the atmosphere and highlighting its pivotal role in modifying the radiation budget. We propose that to upgrade our knowledge on BB aerosol radiative effects in BB source region, the long-term and extensive field measurements are needed.

Keywords: Biomass-burning; Near-source; Aerosol optical properties; Radiative effects; 7-SEAS.

INTRODUCTION

Biomass-burning (BB) aerosols are the significant contributor to the global aerosol loading and radiation budgets (Crutzen and Andreae, 1990; Penner *et al*., 1992). The emissions (i.e., gas and particle) from tropical BB influence the physicochemical and optical properties of the atmosphere (Andreae *et al*., 1988; Crutzen and Andreae, 1990; Andreae and Crutzen, 1997; Hobbs *et al*., 1997; Artaxo *et al*., 1998; Artaxo *et al*., 2001; Andreae and Merlet, 2001; Ramanathan *et al*., 2001; Andreae *et al*., 2002; Artaxo *et al*., 2002; Hobbs *et al*., 2003). BB aerosols affect the radiation budget of the earth and atmosphere by scattering and absorbing directly the incoming solar radiation (e.g., Haywood and Boucher, 2000; Haywood *et al*, 2003a; Myhre *et al*, 2003) and also indirectly by acting as cloud condensation nuclei and changing the cloud microphysical properties (Albrecht, 1989; Twomey, 1977; Haywood and Boucher, 2000; Forster *et al*., 2007). These aerosols can exert either cooling or warming effect on climate, depending on the balance between scattering and absorption (Johnson *et al*., 2008). The capacity of BB aerosols for absorbing and reflecting incident solar radiation mainly depends on the nature of the fuel type, combustion

* Corresponding author.
Tel.: +886-3-422-7151 ext. 65531
E-mail address: nhlin@cc.ncu.edu.tw; carlo@cc.ncu.edu.tw

phase, environmental conditions, and atmospheric aging (Vakkari *et al*., 2014 and references therein). BB aerosols are mainly generated by agricultural burning in tropical regions (Andreae and Merlet, 2001); Africa, the Amazon basin and southern Asia are major source regions (Johnson *et al*., 2008).

The radiative effects of BB particles have remained poorly quantified since their optical and cloud activating properties are very diverse (Vakkari *et al*., 2014). The annual global mean radiative forcing at the top-of-atmosphere (TOA) was estimated as –0.2 W m^{-2} (Intergovernmental Panel on Climate Change (IPCC), 2001) for BB aerosols and with a large uncertainty. Model simulated direct radiative forcing of BB aerosols was found to be +0.03 ± 0.12 W m^{-2} globally (IPCC, 2007). IPCC (2014) reported the radiative forcing of BB aerosols as –0.20 (range; –0.60 to –0.07) W m^{-2} in the Second and Third Assessment Reports, +0.03 (–0.09 to +0.15) W m^{-2} in the Fourth Assessment Report, and 0.0 (–0.20 to +0.20) W m^{-2} in the Fifth Assessment Report. There were a few campaigns conducted to investigate the characteristics of regional BB emitted aerosols and their climatic effect, such as Southern African Regional Science Initiative (SAFARI) (Andreae *et al*., 1996), Smoke, Clouds and Radiation-Brazil (SCAR-B) (Kaufman *et al*., 1998), Indian Ocean Experiment (INDOEX) (Ramanathan *et al*., 2001), Transport and Chemical Evolution over the Pacific (TRACE-P) (Jacob *et al*., 2003), and Biomass Burning Aerosols in Southeast Asia: Smoke Impact Assessment (BASE-ASIA) (Tsay *et al*., 2013). Recently, Pani *et al*. (2016a) reported the enhancement of surface cooling and free troposphere warming by the transported Indochina BB plumes over the northern South China Sea during the Seven South East Asian Studies (7-SEAS)/Dongsha Experiment.

The 7-SEAS/BASELInE (Biomass-Burning Aerosols & Stratocumulus Environment: Lifecycles & Interactions Experiment) was conducted in spring 2013–2015 over northern Southeast Asia to further explore numerous key atmospheric processes and impacts of BB on radiation budgets of surface/atmosphere (Lin *et al*., 2013). BB activities in the form of wildland forest fires and agricultural burning are very pronounced in the northern Indochina regions mainly during dry/spring season from late February to mid-April (i.e., Gautam *et al*., 2013; Hsiao *et al*., 2016). Aerosol concentrations during this season are typically at peak associated with BB activity and contribute significantly to the regional emissions (Carmichael *et al*., 2003; Janjai *et al*., 2009; Streets *et al*., 2009). The impact of BB on air quality over Southeast Asia was evaluated within the framework of BASE-ASIA campaign by using chemical transport modelling (Fu *et al*., 2012; Huang *et al*., 2013). Moreover, some recent studies also emphasized the BB emissions from Indochina region and explained their impact on regional air quality, atmospheric radiation, hydrological cycle, and climate (e.g., Lin *et al*., 2013; Tsay *et al*., 2013; Lin *et al*., 2014; Tsay *et al*., 2016) by using in-situ measurements (e.g., Chuang *et al*., 2013b; Wang *et al*., 2015; Chuang *et al*., 2016; Hsiao *et al*., 2016; Khamkaew *et al*., 2016; Lee *et al*., 2016a; Pantina *et al*., 2016; Sayer *et al*., 2016), satellite observations (e.g., Hsu *et al*., 2003; Huang *et al*., 2011; Campbell *et al*., 2013; Lee *et al*., 2016b), remote sensing (Gautam *et al*., 2013; Reid *et al*., 2013), and modeling studies (Fu *et al*., 2012; Loftus *et al*., 2016) within the 7-SEAS framework. Wang *et al*. (2015) investigated the presence of strongly absorbing (single-scattering albedo ≈0.88 and absorption angstrom exponent ≈1.5) carbonaceous aerosols within the planetary boundary layer (PBL) over northern Indochina in 2014 spring.

The main goal of this work is to assess and quantify the shortwave direct radiative effects over the northern Indochina due to excess loading of near-source BB aerosols during 7-SEAS/BASELInE 2013 campaign (March 1–April 15). Contributions from variety of source regions and aerosol compositions to the total radiative forcing were carefully examined by matching up observational and modeling results. This study provides an better understating on linkage between aerosol surface mass concentration, optical depth and radiative effects of different aerosol components, and can be utilized effectively further in the context of regional and global climate studies.

MEASUREMENTS, DATA, AND METHODOLOGY

Site Description

The study location, Doi Ang Khang meteorology Station [DAK; 19.93°N, 99.05°E, 1536 m above mean sea level (a.m.s.l)], is a high mountain vegetation field in northern Indochina region. The site is near Myanmar border and about 125 km north of Chiang Mai City. It is situated on top of the mountain surrounded by forest and some agricultural fields. The mean synoptic surface winds during spring (March–April) over the Chiang Mai Province, Thailand, where DAK is located, were northwest/west/southwesterly.

Source Region Identification: Back Trajectory Analysis

Five-day back trajectories ending at ground level of DAK at 06 UTC daily study period were calculated using HYSPLIT (Hybrid Single-Particle Lagrangian Integrated Trajectory, Version 4.9) model developed by NOAA Air Resources Laboratory (Draxler and Rolph, 2003) to allocate them in to groups of similar source origin, transport pathways and path length. The meteorological data was obtained from the NCEP Global Data Assimilation System (GDAS) with one-degree resolution and used to initialize HYSPLIT. Three clusters (i.e., Clusters 1–3) were identified over DAK. Individual trajectories representing each cluster are shown in Fig. 1. Cluster 1 (No. of days, N: 15) accounts for 48% of total trajectories and represents the path, originating from Bay of Bengal (BoB) and mostly locally near the source. Trajectories in Cluster 2 (N: 13) accounts for 43%, mainly originated from East-coast India and BoB. Cluster 3 (N: 3) accounts for only 9% of total trajectories and represents the longest path, originating from semi-arid regions over northwest India (NWI) and Indo-Gangetic Plain (IGP) and passing through the coastal areas of Indian subcontinent. Cluster 1 consists of trajectory confined below 2 km, while Cluster 2 and 3 exhibited greater variability with respect to origin heights. All the clusters were mainly influenced by the near-source BB activity.

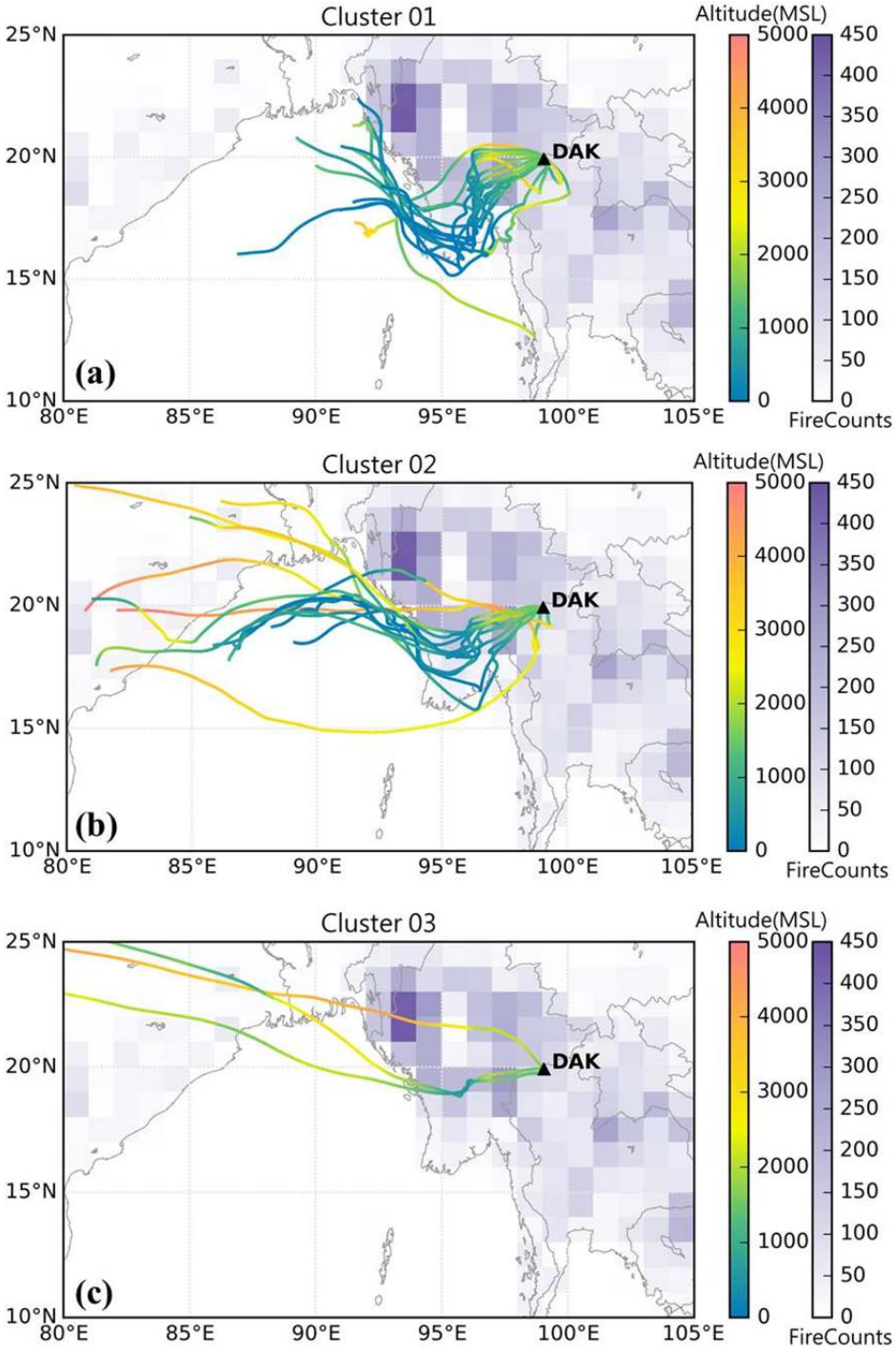

Fig. 1. The location of DAK in northern Indochina. Also shown are the gridded fire counts during March–April 2013 from the MODIS instrument aboard the Terra satellite (http://disc.sci.gsfc.nasa.gov/neespi/data-holdings/mod14cm1.shtml). The 5-day back trajectories ending at ground level of DAK for dates in Clusters 1 to 3 (a–c).

Aerosol Measurements

Measurements of elemental carbon (EC) concentration and total suspended particulate with sizes ≤ 10 μm (PM_{10}) were being carried out at the study location during 01 March–8 April 2013. PM_{10} was collected by using Teflon filters (R2PJ047 TefloTM, PALL Life Sciences, Inc., Ann Arbor, MI, USA) and quartz fiber filters (Tissuquartz 2500 QAT-UP, 20 cm × 25 cm, Pall Corporation, USA) for 24 hours (08:00 a.m. to 08:00 a.m. local time). The collected filters were refrigerated below 4°C before shipping and transported to a laboratory in Taiwan for filter weighting and subsequent analysis. Further water soluble ions (Na^+, NH_4^+, K^+, Mg^{2+}, Ca^{2+}, Cl^-, NO_3^-, and SO_4^{2-}) were analyzed from the Teflon filter sample by an ion chromatograph (DX-120 for cations and DX-1000 for anions, Dionex Co., Inc., Sunnyvale, CA, USA). The quartz fiber filters were analyzed

for EC and organic carbon (OC) fractions by using a DRI Model 2001A OC/EC Carbon Analyzer (Atmoslytic Inc., Calabasas, CA, USA) by the thermal optical reflectance method. More details of the sampling procedure and analytical methods were presented in Chuang *et al*. (2013a, b). Black carbon (BC) is often used interchangeably with EC (Watson *et al*., 2005) and we further used BC throughout in this manuscript.

The aerosol optical properties i.e., aerosol optical depth (AOD), single scattering albedo (SSA), asymmetry parameter (AP), and absorption aerosol optical depth (AAOD) were being obtained from AERONET (AErosol RObotic NETwork) Version 2 Level 2 direct-sun and inversion products. The estimated uncertainty in AOD was 0.01–0.02 and was primarily due to the calibration (Eck *et al*., 1999). Direct-sun data are cloud screened and quality assured based on Smirnov *et al*. (2000), while AERONET inversion products were quality assured based on Dubovik *et al*. (2000) and Holben *et al*. (2006). The uncertainty in the retrieved inversion product was estimated to be ± 0.03 (Holben *et al*., 2006).

Methodology and Criteria of the Study

An aerosol optical model (Optical Properties of Aerosols and Clouds (OPAC 3.1) optical model (Hess *et al*., 1998)) was adopted to calculate aerosol properties by using data from in-situ aerosol measurements as input. The OPAC model can easily incorporate with user defined aerosol mixtures, aerosol vertical profile, wavelength, and relative humidity (RH). The different aerosol components (water insoluble, water soluble, BC, sea salt and mineral dust) were used in the OPAC model based on aerosol source regions and transport pathways over the northern Indochina. Aerosol components used in this study were assumed to be spherical and externally mixed (Koepke *et al*., 1997, Hess *et al*., 1998). Water soluble and sea salt aerosols are predominant scatterers, water insoluble and mineral dust aerosols are absorbers, and BC is the single largest absorber of solar radiation. Atmospheric boundary layer height (the daytime values) obtained from Micro pulse lidar aerosol extinction profiles were used. Detail about the Micro pulse lidar was available in Wang *et al*. (2015). The OPAC works at eight different RH conditions in the range of 0–99% (Hess *et al*., 1998). The measured daily mean value of RH was 50% during the study period and thus used in this study.

Fig. 2 shows the flow diagram describing the methodology for the estimation of aerosol optical properties (AOD, SSA, and AP) in the entire short wave range (0.25–0.4 μm) and direct aerosol radiative effects using measured aerosol parameters (i.e., surface PM_{10} and BC mass concentrations) in the OPAC optical model and a radiative transfer model. The number densities were obtained from the respective mass concentration of individual aerosol components. The number density of different aerosol components (i.e., water insoluble, water soluble, BC, sea salt, and mineral dust) were varied in an iterative process until all the following criteria were satisfied: (1) PM_{10} aerosol surface mass concentration was the same as obtained from observations; (2) BC mass concentration in the OPAC was the same (within ±1) as that

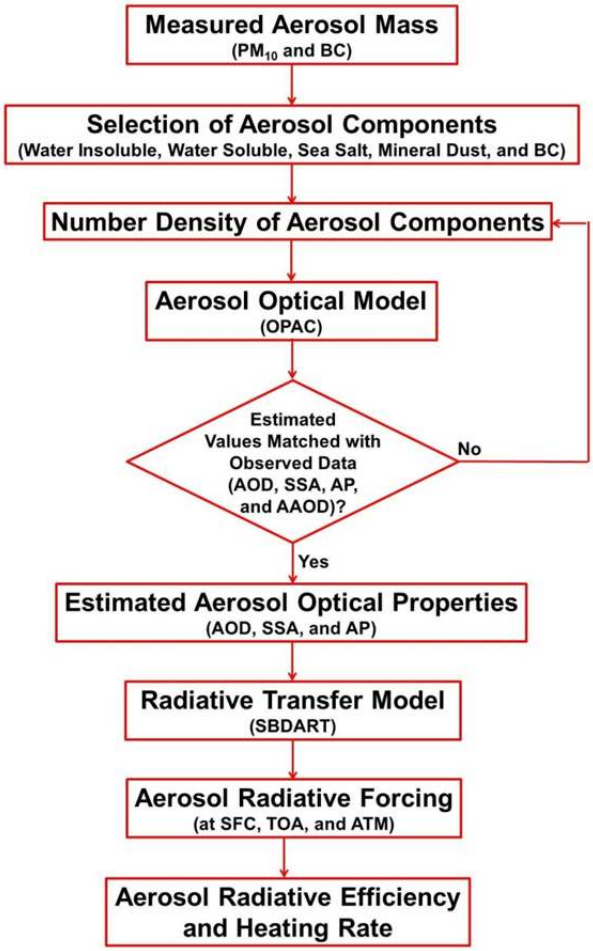

Fig. 2. Flow diagram of the methodology adopted for the estimation of aerosol radiative forcing using SBDART model, in conjunction with the aerosol optical properties estimated from the OPAC in the shortwave (0.25–4 μm) range.

of the chemically measured BC mass; (3) the root-mean-square error between the measured and modeled AOD spectra was < 0.001; (4) model-derived AAOD (sum of AOD due to water insoluble, BC and mineral dust) was matched with AAOD obtained from observations; (5) model-derived SSA was matched with SSA obtained from observations (6) model-derived AP was matched with AP obtained from observations. Furthermore, number density of each aerosol components were used in the OPAC model separately to derive the AOD corresponding to each of the component and their relative contribution to total AOD were also estimated.

By adopting the above methodology, the estimated aerosol optical properties (i.e., AOD, AAOD, SSA, and AP) can be found well matched with the observations as shown in Table 1. Upon the data process, we ensured the constituency between the theoretical and observational results which can further improve the accuracy in radiative transfer calculations.

Aerosol Radiative Effect Estimation

Radiative transfer estimations in the shortwave (0.25–4 μm; 38 bands) range were made by using the SBDART (Santa Barbara DISORT Atmospheric Radiative Transfer)

Table 1. Comparisons of cluster-wise mean aerosol parameters obtained from observations and estimated from model over DAK.

Source/parameters	Cluster 1	Cluster 2	Cluster 3
Observations			
AOD_{500}	0.64 ± 0.27	0.76 ± 0.22	0.81 ± 0.2
$AAOD_{440}$	0.08 ± 0.03	0.10 ± 0.05	0.09 ± 0.06
SSA_{440}	0.89 ± 0.02	0.89 ± 0.02	0.9 ± 0.01
AP_{440}	0.67 ± 0.02	0.67 ± 0.02	0.67 ± 0.02
BC mass (μg m^{-3})	4.4 ± 1.5	5.5 ± 1.5	5.3 ± 1.5
PM_{10} mass (μg m^{-3})	73 ± 26	98 ± 25	104 ± 19
OPAC model			
Total AOD_{500}	0.65	0.76	0.81
$AOD_{Insoluble}$ (a)	0.003	0.003	0.002
$AOD_{Water\ soluble}$	0.55	0.63	0.68
$AOD_{Black\ carbon}$ (b)	0.08	0.09	0.09
$AOD_{Sea\ salt}$	0.02	0.03	0.03
$AOD_{Mineral\ dust}$ (c)	0.00	0.004	0.005
$AAOD_{500}$ (a+b+c)	0.09	0.10	0.09
SSA_{450}	0.89	0.89	0.90
AP_{450}	0.68	0.68	0.68
BC mass (μg m^{-3})	4.4	5.5	5.3
PM_{10} mass (μg m^{-3})	73	98	104

radiative transfer model (Ricchiazzi *et al*., 1998). The radiative transfer equations in this model are numerically integrated with Discreet Ordinate Radiative Transfer (DISORT) radiative transfer module (Stamnes *et al*., 1988). This approach provides a numerically stable algorithm to solve the equations for plane-parallel and non-isothermal radiative transfer in a vertically inhomogeneous atmosphere. The algorithm computes the radiation fluxes for each wave length region in a line-by-line mode with a fixed spectral resolution of 0.005 μm in the shortwave region (Ricchiazzi *et al*., 1998). The radiative transfer calculations were performed using 65 atmospheric layers and 8 radiation streams (8 zenith angles and 8 azimuthal modes) to estimate the upward and downward fluxes at the surface and TOA for 24 hour period (at the interval of 1 hour), with and without aerosols. The fluxes estimated by SBDART model were found to be within 2% of direct and diffuse irradiance measurements (Michalsky *et al*., 2006). This methodology has been widely used in solving the radiative transfer equations and available in literature (e.g., Satheesh, 2002, 2010; Ramachandran *et al*., 2012; Pani, 2013; Srivastava and Ramachandran, 2013). Aerosol radiative forcing (ARF, W m^{-2}) at the surface (ARF_{SFC}) and at the TOA (ARF_{TOA}) was calculated as the change in the net (difference between downward and upward) fluxes with and without aerosol conditions as

$$ARF_{SFC} = (NetFlux)_{\text{with aerosol at SFC}} - (NetFlux)_{\text{without aerosol at SFC}} \quad (1)$$

$$ARF_{TOA} = (NetFlux)_{\text{with aerosol at TOA}} - (NetFlux)_{\text{without aerosol at TOA}} \quad (2)$$

ARF_{ATM}, the amount of energy trapped by the aerosols present in the atmosphere, was estimated as the difference between the ARF_{TOA} and ARF_{SFC}.

Spectral values of aerosol optical properties (AOD, SSA, and AP) at wavelengths of 0.25–4 μm obtained from OPAC optical model for each cluster measurement were incorporated in SBDART to estimate ARF in clear sky. ARF corresponding to each aerosol components for each cluster were also calculated by taking the difference between ARF_{Total} (Eqs. (1) and (2)) and the ARF in absence of that particular component. In addition to aerosol optical properties, the atmospheric profiles of temperature, pressure, columnar ozone, water vapor and surface reflectance were also required in SBDART model to compute ARF. The standard tropical atmospheric profiles of temperature and pressure, as described in Ricchiazzi *et al*. (1998), were used in this study. The tropical climate is characterized by the average water vapor (4.1 g cm^{-2}) and the average ozone level (253 Dobson Unit). SBDART model also includes the default values for the trace gases CO_2 (360 parts per million; ppm), CH_4 (1.74 ppm), and N_2O (0.32 ppm). Surface reflectance is a crucial factor in determining the strength of ARF. Gautam *et al*. (2013) reported the composite mean map of CERES (Clouds and the Earth's Radiant Energy System) derived broadband surface reflectance during February–April over Indochina region in the 0.12–0.16 range indicating low surface albedo over the largely vegetated regions. SBDART uses the default value of surface reflectance as 0.127 at 555 nm for vegetation (Manual of Remote Sensing, 1975) surface type. Moderate Resolution Imaging Spectroradiometer (MODIS) derived land surface products (Moody *et al*., 2005) like black-sky albedo (direct reflectance) and white-sky albedo (bi-hemispherical reflectance) were used to model the surface reflectance (e.g., Satheesh *et al*., 2010; Campbell *et al*., 2016) characteristics required for the radiative transfer calculation. MODIS surface reflectance data were obtained at seven different wavelengths centered at 469, 555, 645, 858.5, 1240, 1640, and 2130 nm and used to reproduce the

surface reflectance in the entire short wavelength spectrum using a combination of water, sand, and vegetation surface types (e.g., Ramachandran *et al*., 2012; Pani, 2013; Verma *et al*., 2013). The spectral mean surface reflectance over DAK was obtained as 0.123. The combination of water (3%), sand (0%), and vegetation (97%) was made in appropriate proportions such that the resultant spectrum matched the MODIS derived surface reflectance.

The aerosol radiative efficiency (ARE), change in ARF per unit AOD at 500 nm, was also estimated. The ARF_{ATM} in the shortwave region gets converted into heat and the heating rate at each layer (ΔP) is given by

$$\frac{\partial T}{\partial t} = \frac{g}{C_p} \times \frac{ARF_{ATM}}{\Delta P} \quad (3)$$

where ($\Delta T/\partial t$) is the heating rate (Kelvin per day; K d^{-1}), g is the acceleration due to gravity (9.8 m s^{-1}), C_p is the specific heat capacity of air at constant pressure (1006 J kg^{-1} K^{-1}), and P is the atmospheric pressure difference (Liou, 1980). ΔP was considered as 200 hPa (equal to the pressure difference between ground and 3.5 km) in this study.

RESULTS AND DISCUSSIONS

Aerosol Vertical Profiles

Aerosol vertical profiles from lidar observations were analyzed to determine the aerosol vertical distribution over DAK and used in this study. The mean aerosol extinction profile for the entire study period is shown in Fig. 3. The height of aerosol vertical distribution reached 5 km a.m.s.l was attributed to PBL dynamic over mountain area and transported aerosol plume (Wang *et al*., 2015). The peak of the mean aerosol extinction (0.37 km^{-1}) was observed between 2.5 km to 3.5 km a.m.s.l indicating the presence of lofted aerosol layer.

Measured Properties of Aerosol: Day-to-Day Aerosol Variability

The PM_{10} and BC mass concentrations over DAK were ranged between 25–135 µg m^{-3} (mean ± one standard deviation; 87 ± 28 µg m^{-3}) and 5–10 µg m^{-3} (7 ± 2 µg m^{-3}), respectively during the entire study period. The measured PM_{10} and BC mass concentrations were strongly correlated (R^2 = 0.8) over DAK and suggested the common source origins. Fig. 4 shows the daily variations in various aerosol optical properties obtained from the AERONET observations. The columnar integrated AOD represents the extinction of incoming solar radiation by aerosols and its magnitude is directly proportional to the loading of aerosols in the total atmospheric column. The columnar AOD_{500} (Fig. 4(a)) was found to be from 0.26 to 1.13 (0.71 ± 0.24) during the study period.

The spectral dependence of the AOD was used to compute the Angstrom exponent (AE). AE is also a qualitative indicator for the size of aerosol particles (Pani and Verma, 2014). The variations in the magnitude of $AE_{440/870}$ were shown in Fig. 4(b), which was found to vary from 1.64 to 1.95 (with a mean 1.77 ± 0.07). The results suggested the relative dominance of smaller aerosols over the region, mainly from the BB emissions. Fig. 4(c) shows daily average fine mode fraction (FMF), observed at 500 nm wavelength during the period of study. Predominant contribution from fine mode aerosol was clearly observed and the FMF_{500} ranged between 0.88–0.98 (with a mean 0.95 ± 0.02). The

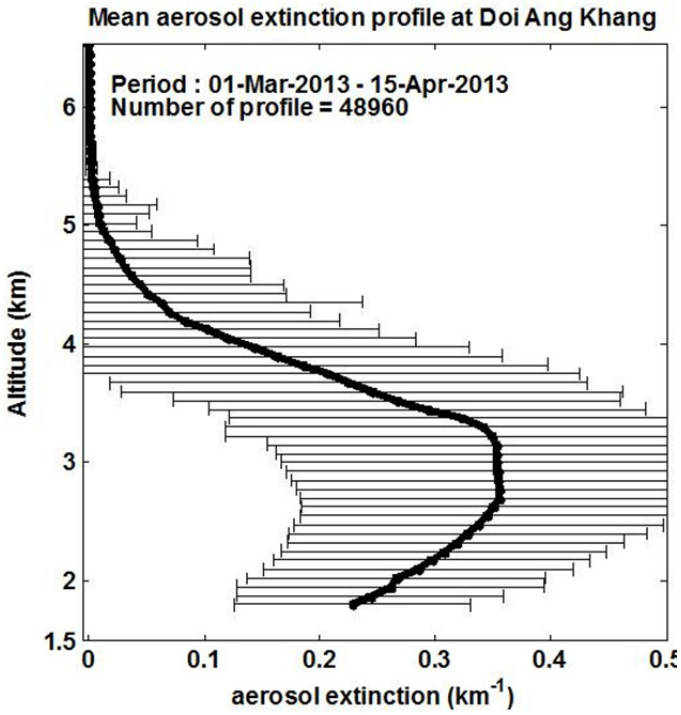

Fig. 3. Mean aerosol extinction profile with standard deviation during March 1 and April 15, 2013 over DAK.

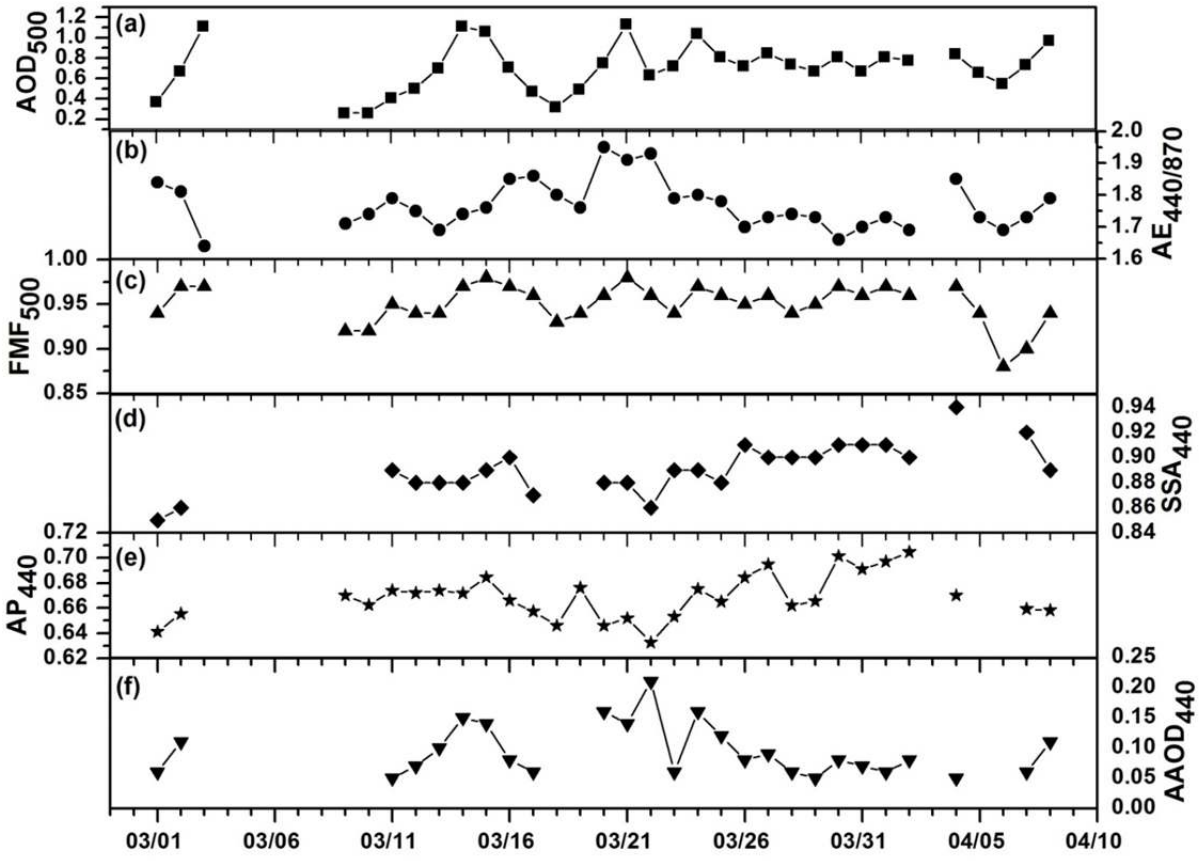

Fig. 4. Day-to-day variation in observed aerosol optical properties (a) AOD at 500 nm, (b) AE at 440 and 870 nm, (c) FMF at 500 nm, (d) SSA at 440 nm, (e) AP at 440 nm, and (f) AAOD at 440 nm over DAK during the entire study period.

mean fine mode and coarse mode AOD at 500 nm (not shown in figure) was 0.67 ± 0.23 (0.24–1.1) and 0.03 ± 0.01 (0.02–0.06), respectively during the study period.

The SSA is a very common and crucial measure of the relative contribution of absorption to total extinction and also a key parameter in climatic assessment of effects of aerosols (Jacobson, 2000; Dubovik *et al*., 2002). It is the ratio of scattering coefficient to the extinction coefficient (the sum of scattering and absorption coefficient). SSA_{440} (Fig. 4(d)) varied in between 0.85–0.94 (with a mean 0.89 ± 0.02) over DAK and suggested the dominance of BB aerosols. Wang *et al*. (2015) reported the presence of strongly absorbing (SSA_{440} ≈0.88) smoke particles over northern Indochina in 2014 spring. It was also observed that SSA decreases with wavelength (SSA_{440} ≈0.89) and SSA_{1020} ≈0.84). Higher SSA at shorter wavelength indicates the dominance of absorbing aerosols mainly attributed to near-source BB emissions. Long-range transport of dust/pollutants from NWI/IGP to the DAK may also play a role here. The SSA_{440} over DAK was very close to the value observed in Senanga, Zambia (0.86), Mwinilunga, Zambia (0.88), Skukuza, South Africa (0.88), Etosha Pan, Namibia (0.90), Inhaca Island, Mozambique (0.88) and Bethlehem, South Africa (0.90) during SAFARI 2000 dry season (August–September) campaign in southern Africa (Eck *et al*., 2003). The SCAR-B experiment in Brazil measured SSA as low as 0.6 (at 550 nm wavelength) for fresh smoke (Reid *et al*., 1998) and increasing up to 0.91 as the smoke aged. Measurements of Canadian smoke during the Boreal Ecosystem-Atmosphere Study (BOREAS) found SSA in range from 0.70 for fresh smoke to 0.98 for aged smoke (Miller and O'Neill, 1997; Li and Kou, 1998).

The AP is the measure of angular distribution of light scattered by the aerosol particles and gives information on aerosol size and scattering properties (Andrews *et al*., 2006). It is another key parameter which regulates aerosol radiative forcing. However ARF is less sensitive to changes in AP when compared to AOD and SSA (Srivastava and Ramachandran, 2013). The daily variations in AP_{440} (Fig. 4(e)) was opposite to the variations in AE (with R^2 = 0.55). AP_{440} varied in between 0.63–0.70 (with a mean 0.67 ± 0.02) over DAK. AAOD, a measure of the column aerosol light absorption, is expressed as AOD × (1 – SSA). $AAOD_{440}$ (Fig. 4(f)) was varied in between 0.05–0.21 (with a mean 0.10 ± 0.04) during the entire study period and showed a moderate absorption over the study site. The highest AAOD (0.21) was observed on March 22 (SSA ≈ 0.86) and the lowest AAOD (0.05) was on April 4 (SSA ≈ 0.94).

Table 2 shows the aerosol optical properties of BB aerosols from the different AERONET sites over the BB regions of Amazon (Alta Floresta and Cuiaba), Australia (Jabiru), Boreal (Bonanza Creek, Moscow, Tomsk 22, and Yakutsk) forest, Savanna (Skukuza and Mongu), and Indochina (Mukdahan, Maesoon, Luang Namtha, Sonla, and DAK) regions.

Table 2. Aerosol optical properties from worldwide BB source regions.

Place	Region	Fire type	Latitude (N)	Longitude (E)	Elevation (m)	BB season	Periods	SSA_{440}	AP_{440}	$AE_{440/870}$	References
Alta Floresta	Amazon	Forest	–9.871	–56.10	277	Aug.–Oct.	1999–2011	0.92	0.68	1.95	Sayer *et al.*, 2014
Cuiaba	Amazon	Forest	–15.729	–56.02	210	Sept.– Oct.	2001–2013	0.89	0.68	1.91	Sayer *et al.*, 2014
Jabiru	Australia	Forest	–12.66	132.89	30	--	2003–2012	0.88	0.69	1.88	Sayer *et al.*, 2014
Bonanza Creek	North America	Boreal Forest	64.74	–148.32	150	Apr.–Sept.	1999–2012	0.95	0.69	1.42	Sayer *et al.*, 2014
Moscow	Russia	Boreal Forest	55.70	37.51	199	June–Sept.	2002, 2010	0.95	0.70	1.62	Sayer *et al.*, 2014
Tomsk 22	Russia	Boreal Forest	56.42	84.07	80	Apr.–Sept.	2011–2013	0.94	0.70	1.54	Sayer *et al.*, 2014
Yakutsk	Russia	Boreal Forest	61.66	129.37	118	Apr.–Sept.	2004–2013	0.95	0.69	1.74	Sayer *et al.*, 2014
Skukuza	South Africa	Savanna	–24.99	31.59	150	July–Oct.	1999–2010	0.90	0.68	1.97	Sayer *et al.*, 2014
Mongu	Africa	Savanna	–15.25	23.15	1107	July–Oct.	1999–2009	0.87	0.67	1.89	Sayer *et al.*, 2014
Mukdahan	Indochina	Forest and agricultural	16.60	104.68	166	Feb.–Apr.	2004–2009	0.91	0.71	1.66	Sayer *et al.*, 2014
Maesoon	Indochina	Forest and agricultural	19.83	99.17	502	Mar.– Apr.	2014	0.86	0.67	1.75	Wang *et al.*, 2015
Luang Namtha	Indochina	Forest and agricultural	20.93	101.42	557	Mar.–Apr.	2014	0.86	0.68	1.73	Wang *et al.*, 2015
Son La	Indochina	Forest and agricultural	21.33	103.91	683	Mar.–Apr.	2014	0.89	0.69	1.69	Wang *et al.*, 2015
DAK	Indochina	Forest and agricultural	19.93	99.05	1536	Mar.–Apr.	2014	0.89	0.67	1.73	Wang *et al.*, 2015
DAK	Indochina	Forest and agricultural	19.93	99.05	1536	Mar.–Apr.	2013	0.89	0.67	1.77	This study

Compared with results from Sayer *et al*. (2014) and Wang *et al*. (2015), higher values and similar trend in $AE_{440/870}$ was seen for BB aerosols over Amazon (≈1.9–2.0) basin, Savanna (≈1.9–2.0) forest, and Australia (≈1.9) followed by Indochina (≈1.7–1.8) and Boreal forests (≈1.4–1.7) of North America and Russia. The SSA440 (as shown in Table 2) for smoke varied notably (ranging from 0.86 to 0.95) over distinct BB regions in the world. SSA_{440} was marked the lowest over Indochina (0.86–0.91) followed by Savanna (0.87–0.9), Australia (0.88), Amazon (0.89–0.92), and Boreal (0.94–0.95). The boreal forest demonstrated the weakest aerosol absorption. Indochina smoke exhibited the strongest absorption (lowest SSA value) among Savanna, Amazon, northern Australia and Boreal smoke. Moreover a little stronger absorption ($SSA_{440} \approx 0.86$) was observed over the Thai-Laos valley (Maesoon and Luang Namtha) than that of other Indochina (Mukdahan, Sonla, and DAK) regions (SSA_{440} of 0.89–0.91 or ~0.9). Aerosol absorption ($SSA_{440} \approx 0.89$, $AP_{440} \approx 0.67$ and $AE_{440/870} \approx 1.7$) was observed closely similar during spring of 2014 and 2013 over DAK. As stated in the comparison Table 2, we can conclude that the optical properties of BB aerosols over northern Indochina are distinct from those over other BB regions by taking everything into account.

Cluster Variability

Cluster-wise AOD_{500} showed a strong variation with the trend similar to PM_{10} mass concentrations (Table 1) over the study region. The AOD (PM_{10}) was 0.64 (73 μg m^{-3}), 0.76 (98 μg m^{-3}), and 0.81 (104 μg m^{-3}) for Clusters 1, 2, and 3 respectively. The highest value AOD (0.81) was observed for Cluster 3, with the highest SSA_{440} (0.9) due to the relatively more influence of sea salt from BoB and mineral dust from NWI/IGP region to the study site. $AAOD_{440}$ also showed a distinct cluster variation and the trend was similar to the mean BC mass. The $AAOD_{440}$ (BC) was 0.08 (4.4 μg m^{-3}), 0.1 (5.5 μg m^{-3}), and 0.09 (5.3 μg m^{-3}) for Clusters 1, 2, and 3 respectively mainly due to the presence of absorbing carbonaceous aerosols over DAK. The highest $AAOD_{440}$ was recorded for Cluster 2 with the highest BC (5.5 μg m^{-3}) and $AE_{440/870}$ (1.79) values suggesting the presence of more fresh smoke particles in Cluster 2.

Modeled Properties of Aerosol: Relative Contribution of Different Components to Total Mass

Magnitude of net aerosol radiative forcing depends on both absolute mass concentration of individual components like BC and its mass fraction in total aerosol loading (Petzold *et al*., 1997). Estimated cluster mean relative contribution of different aerosol components to total aerosol mass (Figs. 5(a), 5(b) and 5(c)) concentration reveals a larger variability in water soluble (77–83%), mineral dust (0–5%) components than that in water insoluble (4–7%), sea salt (4–7%), and BC (5–6%). The highest contribution of water soluble (which is optically scattering in nature and made up of various kinds of sulfates, nitrates, organics, etc.) aerosols to the total aerosol mass concentration was estimated and mainly attributed to frequent BB activities in spring. BB aerosols grow by coagulation, condensation and other gas-to-particle

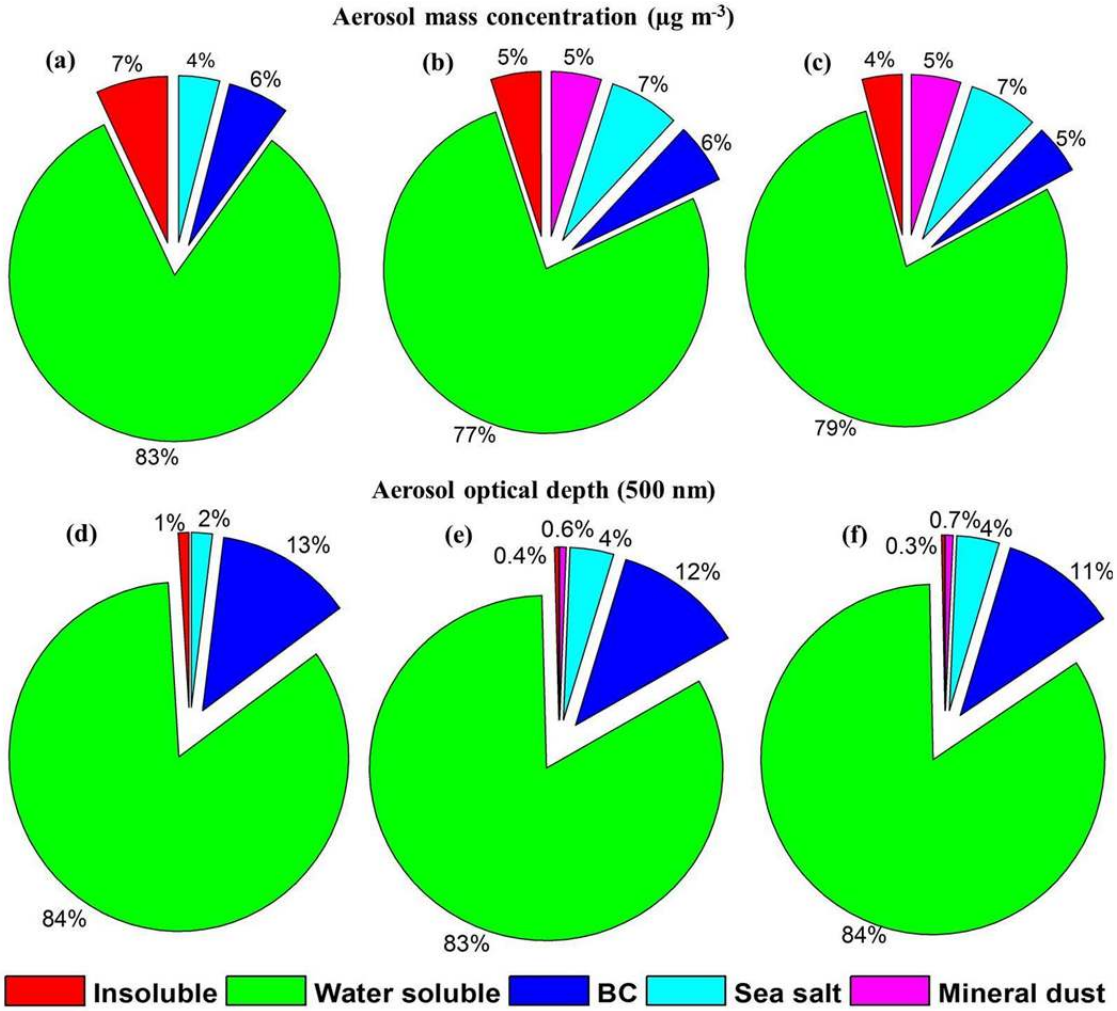

Fig. 5. Percentage contribution of aerosol components to total aerosol mass (μg m^{-3}) obtained from the OPAC for (a) Cluster 1 (73 ± 26), (b) Cluster 2 (98 ± 25), and (c) Cluster 3 (104 ± 19). Percentage contribution of aerosol components to total AOD_{500} obtained from the OPAC for (d) Cluster 1 (0.64 ± 0.27), (e) Cluster 2 (0.76 ± 0.22), and (f) Cluster 3 (0.81 ± 0.2).

exchanges (Jhonson *et al*, 2008) with time. Aerosol ageing increases the scattering coefficient and single scattering albedo (Reid *et al*., 1998; Abel *et al*., 2003). It is worthy to be noted that, since an exact match was obtained between the observations and the model estimated optical properties, so any impact due to internal mixes (core-shell or homogeneous mixing) of aerosols on the aerosol optical properties and radiative estimations were non-significant (Ramachandran *et al*., 2012). Water soluble contribution was the highest (83%) for Cluster 1 mainly due to the influence of local BB aerosols, followed by for clusters 2 (77%) and 3 (79%) due to the contribution of sea salt and mineral dust aerosols. Water insoluble (mainly suspended soil/road dust particles with a certain amount of organics matter) aerosols contributed the highest (7%) for Cluster 1. BC aerosols contributed the highest (6%) to the total aerosol mass for Cluster 1, mainly because of local and near-source BB activities. Sea salt aerosols contributed the lowest (4%) in Cluster 1, while relatively higher (7%) for Clusters 2 and 3, as aerosols were coming over BoB to the study site. No dust contribution was estimated for Cluster 1 but 5% for both the Clusters 2 and 3 as the influence of aerosols from NWI and IGP region of Indian subcontinent. SSA was relatively lower (0.89) for Clusters 1 and 2 owing to the dominance of fine mode absorbing aerosols. SSA was the highest (0.9) for Cluster 3 due to the increase in the abundance of sea salt aerosols which are more scattering in nature.

Relative Contribution of Different Components to Total AOD

AOD_{500} due to different aerosol components (i.e., water insoluble, water soluble, BC, sea salt and mineral dust) for Clusters 1–3 were estimated in the OPAC model and presented in Table 1. Furthermore their relative contributions to total AOD (Figs. 4(d), 4(e), 4(f)) were also estimated. Cluster mean aerosol component AOD exhibits a low variability compared to their mass concentrations. The AOD due to water soluble aerosols (component AOD: 0.55–0.68; relative contribution to the total AOD: 83–84%) was predominant over DAK, followed by that due to BC (0.08–0.09; 11–13%), sea salt (0.02–0.03; 2–4%), mineral dust (0.004–0.005; 0.55–0.58%), and water insoluble (0.002–

0.003; 0.3–0.5%) aerosols during the study period. Water soluble aerosols and BC contributed as high as 97% to total AOD for Cluster 1, followed by Clusters 2 and 3 (95%). Sea salt contribution to AOD was maximum 4% for Clusters 2 and 3 and only 2% for Cluster 1. The contribution of mineral dust was 5% to the total aerosol mass for Clusters 2 and 3, but its contribution to the total AOD was very little (0.6%). Negligible contribution of water insoluble component to total AOD was observed. The BC only contributed 5–6% to the aerosol mass loading, but its contribution to the total AOD was 11–13% (≈2 times higher). This showed the importance of BC aerosol mass fraction on the optical and radiative effect over near source BB region. Though the BC aerosol was present only in very small fractions, their effect on short wave radiation was significant.

Clear-Sky Shortwave Direct Aerosol Radiative Effects

The magnitude of estimated shortwave total ARF (ARF_{TOA}, ARF_{SFC}, and ARF_{ATM}) estimated from aerosol optical properties for each clusters is given in Table 3. The cluster variation in ARF over DAK was not so significant because of the similar contribution from the water soluble and BC aerosols. ARF_{TOA} and ARF_{SFC} for Clusters 1–3 were ranged between –7.1 to –9.1 and –28.3 to –33.5 W m^{-2}, respectively. Variations in ARF were mainly due to the variations in AOD and SSA (Ramachandran *et al*., 2012; Pani *et al.* 2016b). Cluster 3 showed the highest ARF (ARF_{TOA} of –9.1 W m^{-2} and ARF_{SFC} of –33.5 W m^{-2}) due to the highest AOD_{500} (0.81) and SSA_{440} (0.9) as well. The model simulated monthly mean ARF_{TOA} of BB aerosols in the southern African region during SAFARI-2000 was found to be –4.3 W m^{-2} (Myhre *et al*. 2003). The mean ARF_{TOA} during the BB season (August and September) for the 10-yr (2000 to 2009) was –5.6 ± 1.7 W m^{-2} over Amazonia (Sena *et al*., 2013). The overall mean ARF_{TOA} value (–8.0 W m^{-2}; see Table 3) over Indochina was 1.4 times higher than that over Amazonia. Table 4 shows that the mean daily ARF_{TOA} results over the Amazon Basin were compatible with this present study. ARF_{ATM} (+24.7 W m^{-2}) was the highest for the Cluster 2 due to the highest BC (5.5 μg m^{-3}) and $AAOD_{440}$ (0.1) as well.

The ARF (ARF_{TOA}, ARF_{SFC}, and ARF_{ATM}) values due to individual aerosol components for all clusters are shown in Fig. 6. ARF_{SFC} values were negatives for each component. ARF_{SFC} was the highest for water soluble (–17.5 to –21.2 W m^{-2}) followed by BC (–17.6 to –18.7 W m^{-2}), sea salt (–0.3 to –0.7 W m^{-2}), water insoluble (–0.2 to –0.3 W m^{-2}), and mineral dust (–0.2 to –0.3 W m^{-2}). Absorbing aerosols (water insoluble and BC) only showed positive values at TOA, whereas scattering aerosols (water soluble and sea salt) showed negative values. BC aerosols showed warming of +10.2 to +11.1 W m^{-2} at TOA and water soluble (–9.6 to –11.5 W m^{-2}) balanced the effect. ARF_{ATM} was +27.8 to +29.8 W m^{-2} due to BC aerosols along with negligible contribution from water insoluble (+0.3 to +0.4 W m^{-2}) and mineral dust (+0.2 to +0.3 W m^{-2}). BB aerosols (mainly water soluble and BC) were the main contributor to the ARF values, while others were negligible mainly due to their low extinction efficiency.

ARE is a useful parameter for quantifying and comparing aerosol radiative effects at different places under different aerosol conditions (Satheesh and Ramanathan, 2000). The mean values of total ARE_{TOA} (ARE_{SFC}) were –11.1 (–44.2), –10.4 (–42.8), and –11.2 (–41.3) W m^{-2} for Clusters 1, 2, and 3, respectively (Table 3). ARE_{TOA} values were –15.7 ± 2.4 and –9.3 ± 1.7 W m^{-2} over forest and savannah-like vegetation, respectively over Amazonia (Sena *et al*., 2013). Table 4 also shows the mean daily ARE_{TOA} results over the Amazon Basin. The slight deviations in ARE_{TOA} over Amazon and Indochina are mainly due to the difference in BB aerosol loading over two different geographical regions. The mean daily ARE_{TOA} values obtained for Cerrado regions

Table 3. Summary of radiative effects over DAK.

Parameters	Total ARF (W m^{-2})			Total ARE (W m^{-2} per unit AOD_{500})			Heat rate (K d^{-1})	
	ARF_{TOA}	ARF_{ATM}	ARF_{SFC}	ARE_{TOA}	ARE_{ATM}	ARE_{SFC}	Total	BC
Cluster 1	–7.1	+21.2	–28.3	–11.1	+33.1	–44.2	1.0	1.4
Cluster 2	–7.9	+24.7	–32.6	–10.4	+32.5	–42.8	1.2	1.5
Cluster 3	–9.1	+24.4	–33.5	–11.2	+30.1	–41.3	1.2	1.4
Overall mean	–8.0	+23.4	–31.4	–10.9	+31.9	–42.8	1.1	1.4

Table 4. Comparison of BB aerosols ARF from this study with literatures.

Region	Period	ARF_{TOA} (W m^{-2})	ARE_{TOA} (W m^{-2})	References
Amazon	Aug.–Sep., 2002–2009	–5.6 ± 1.7	–13.1 ± 1.6	Sena *et al*., 2014
Amazon	Aug.–Sep., 2000–2005	–7.6 ± 1.9	--	Patadia *et al*., 2008
Amazon	Aug.–Sep., 2002	–5.6 ± 0.6	–10.5	Procopio *et al*., 2004
Alta Floresta, Amazon	Aug.–Sep., 1993–2002	–8.3 ± 2.0	--	Procopio *et al*., 2004
Abracos Hill	Aug.–Sep., 1994–2002	–8.4 ± 2.2	--	Procopio *et al*., 2004
Forest, Amazon	Aug.–Sep., 2000–2009	–6.2 ± 1.9	–15.7 ± 2.4	Sena *et al*., 2014
Forest, Amazon	Aug.–Sep.,1995	--	–20 ± 7	Ross *et al*., 1998
Cerrado, Amazon	Aug.–Sep., 2000–2009	–4.6 ± 1.6	–9.3 ± 1.7	Sena *et al*., 2014
Cerrado, Amazon	Aug.–Sep.,1995	--	–8 ± 9	Ross *et al*., 1998
Indochina (DAK)	Mar.–Apr., 2013	–8.0 ± 1.0	–10.9 ± 0.4	This study

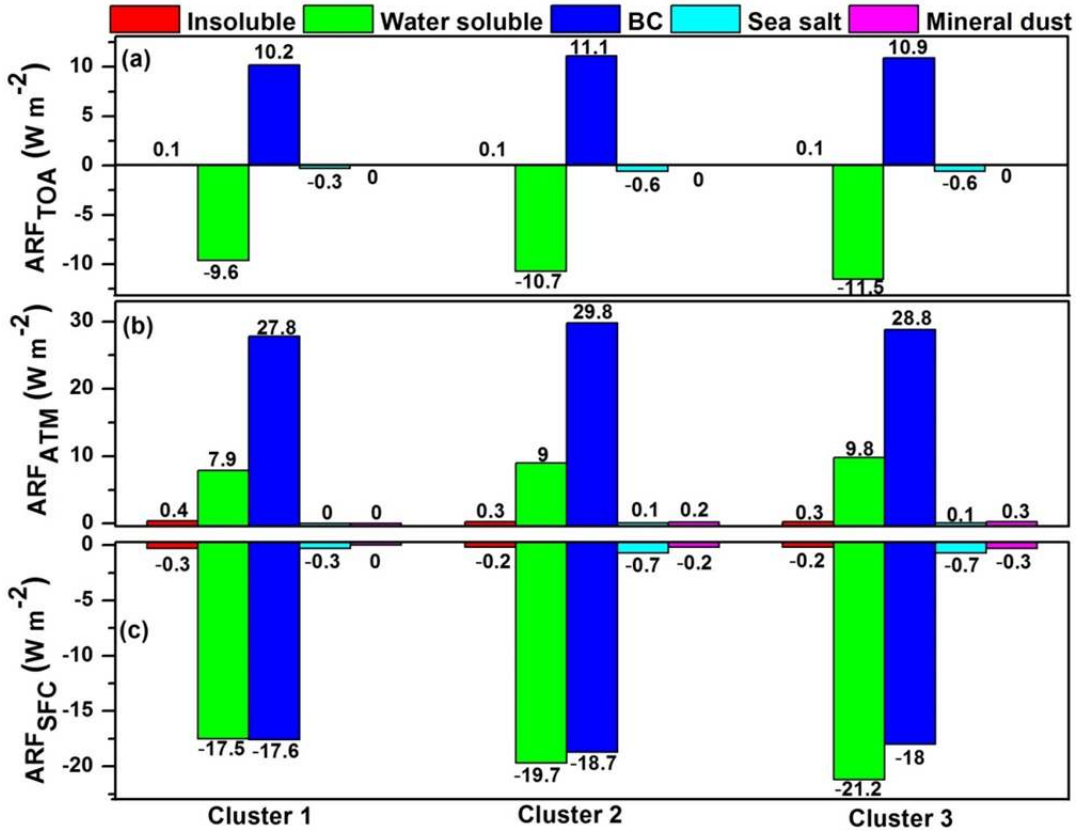

Fig. 6. ARF due to aerosol components (water insoluble, water soluble, BC, sea salt and mineral dust) (a) at TOA, (b) at atmosphere, and (c) at surface, for Clusters 1, 2, and 3 over DAK. The numbers over each bar represents the value of forcing in W m^{-2}.

were much compatible with our results. Also it is very interesting to note that ARE_{TOA} (–10.5 W m^{-2}) over Amazon in 2005 (Procopio *et al*., 2004) was nearly close with our result (–10.9 W m^{-2}) over Indochina. Furthermore, value of the cluster mean atmospheric heating rate (estimated by Eq. (3)) was ranged between 1–1.2 and 1.4–1.5 K d^{-1} due to total and BC aerosols (Table 3), respectively.

This present study showed that radiative impacts of aerosols were more dependent on AOD and SSA rather than their surface mass concentrations. A sensitivity analysis was also carried out to understand the uncertainty in the ARF estimated by the SBDART model. The uncertainty in ARF was calculated by constantly running the model by varying the value of AOD and SSA while keeping all other input parameters unchanged. It was estimated that an error of 0.02 in AOD can result the uncertainty of 2–4% and 5–8% in ARF_{TOA} and ARF_{SFC}, respectively. Likely, an error of 0.01 in SSA can result the uncertainty of 10–15% and 10% in ARF_{TOA} and ARF_{SFC}, respectively. However, the uncertainty value reported in this study is consistent with some earlier reported literature (e.g., Ramachandran *et al*., 2012; Srivastava and Ramachandran, 2012). Also our results revealed that the ARF is mainly governed by the BB aerosols, which contributed up to ≈50% to the ARF_{SFC} and significantly contributing to solar dimming. The contribution of BC aerosols towards ARF_{ATM} was up to ≈75% during the BB season over Indochina. The large negative ARF_{SFC} and positive ARF_{ATM} estimated in this study can have a significant influence on atmospheric stability and regional climate. Our measurements were carried out over mountain top and there is valley with scattering agriculture. Moreover, northern Indochina is a complex terrain and has a high prevalence of forest-conversion fires. So the radiative impact will be larger when we will consider more topography effects, and it should be an appealing topic for future study.

CONCLUSIONS

In this study, we evaluated aerosol radiative impacts of BB aerosols over near-source BB emission region in northern Indochina by using ground-based physical, chemical, and optical data obtained from the 7-SEAS/BASELInE in 2013 as well as by using aerosol optical and radiative transfer models. We analyzed data from in-situ measurements, and trajectory simulations, to explore the relationships between the origins and transport of atmospheric pollutants over northern Indochina. Cluster analysis of back trajectories revealed the mainly contribution from near-source origins for Cluster 1 followed by Cluster 2 and Cluster 3 (influence of mineral dust from Indian subcontinent or NWI/IGP). The mean PM_{10} and EC mass concentrations were ranged between 25–135 μg m^{-3} (87 ± 28 μg m^{-3}) and 5–10 μg m^{-3} (7 ± 2 μg m^{-3}), respectively. Cluster variations in PM_{10} (BC) mass was 73 ± 26 μg m^{-3} (4.4 ± 1.5 μg m^{-3}), 98 ± 25

μg m^{-3} (5.5 ± 1.5 μg m^{-3}), and 104 ± 19 μg m^{-3} (5.3 ± 1.5 μg m^{-3}), for Cluster 1, 2, and 3, respectively.

The columnar AOD_{500} was found to be ranged from 0.26 to 1.13 (0.71 ± 0.24). The optical properties of BB aerosols owing to the dominance of fine mode ($FMF_{500} \approx 0.95$, $AE_{440/870} \approx 1.77$) and strong absorbing aerosols (columnar $SSA_{440} \approx 0.89$, $AP_{440} \approx 0.67$, $AAOD_{440} \approx 0.1$) over northern Indochina. AOD variations between Clusters 1–3 was 0.64, 0.76, and 0.81 and found consistent with the mean PM_{10} mass concentrations. Similarly the $AAOD_{440}$ was 0.08, 0.1, and 0.09 for Clusters 1, 2, and 3, respectively and found consistent with the mean BC (absorbing carbonaceous aerosols) surface mass.

BB aerosols (water soluble and BC) were found mainly predominate in both surface mass concentration and the in columnar burden over the northern Indochina in spring. Water soluble aerosols contributed as high as 80% and 83% to surface mass and AOD_{500}, respectively. BC aerosols contributed only 6% to surface aerosol mass, but its contribution to the total AOD was 12% (2 times higher). ARF variations in Clusters 1–3 was mainly due to the variations in AOD and SSA. The overall mean ARF_{TOA} and ARF_{SFC} were –8.0 and –31.4 W m^{-2}, respectively. The mean ARF_{TOA} and ARF_{SFC} were +10.7 and –18.1 W m^{-2}, respectively due to BC aerosols with the heating rate of 1.4 K d^{-1}. The contribution of BC aerosols towards ARF_{ATM} was up to 75% over Indochina region and draw special attention to its pivotal role in modifying the radiation budget and regional climate. Thus the results gain further interest to understand the large spatial and temporal variations in BB aerosol loading, their sources and radiative impacts over this region.

ACKNOWLEDGMENTS

This work was supported by the Ministry of Science and Technology of Taiwan (MOST 103-2111-M-008-001 and 104-2111-M-008-002) and by the Taiwan Environmental Protection Administration (EPA-104-U1L1-02-101). The 7-SEAS/BASELInE, MPLNET and AERONET project was supported by the NASA Earth Observing System and Radiation Sciences Program. The authors also gratefully acknowledge the NOAA Air Resources Laboratory for the provision of the HYSPLIT transport and dispersion model used in this publication.

REFERENCES

Abel, S.J., Haywood, J.M., Highwood, E.J., Li, J. and Buseck, P.R. (2003). Evolution of biomass burning aerosol properties from an agricultural fire in southern Africa. *Geophys. Res. Lett*. 30: 1783.

Albrecht, B.A. (1989). Aerosols, cloud microphysics, and fractional cloudiness. *Science* 245: 1227−1230.

Andreae, M.O., Browell, E.V., Garstang, M., Gregory, G.L., Harriss, R.C., Hill, G.F., Jacob, D.J., Pereira, M.C., Sachse, G.W., Setzer, A.W., Dias, P.L.S., Talbot, R.W., Torres, A.L. and Wofsy, S.C. (1988). Biomass-Burning Emissions and Associated Haze Layers over Amazonia. *J. Geophys. Res*. 93: 1509–1527.

Andreae, M.O., Fishman, J. and Lindesay, J. (1996). The Southern Tropical Atlantic Region Experiment (STARE): Transport and Atmospheric Chemistry near the Equator-Atlantic (TRACE A) and Southern African Fire-Atmosphere Research Initiative (SAFARI): An introduction. *J. Geophys. Res*. 101: 23519–23520.

Andreae, M.O. and Crutzen, P.J. (1997). Atmospheric aerosols: Biogeochemical sources and role in atmospheric chemistry. *Science* 276: 1052–1058.

Andreae, M.O. and Merlet, P. (2001). Emission of trace gases and aerosols from biomass burning. *Global Biogeochemical Cycles*. 15: 955–966.

Andreae, M.O., Artaxo, P., Brandao, C., Carswell, F.E., Ciccioli, P., da Costa, A.L., Culf, A.D., Esteves, J.L., Gash, J.H.C., Grace, J., Kabat, P., Lelieveld, J., Malhi, Y., Manzi, A.O., Meixner, F.X., Nobre, A.D., Nobre, C., Ruivo, M., Silva-Dias, M.A., Stefani, P., Valentini, R., von Jouanne, J. and Waterloo, M.J. (2002). Biogeochemical cycling of carbon, water, energy, trace gases, and aerosols in Amazonia: The LBAEUSTACH experiments. *J. Geophys. Res.* 107: 8066.

Andrews, E., Sheridan, P.J., Fiebig, M., McComiskey, M., Ogren, J.A., Arnott, P., Covert, D., Elleman, R., Gasparini, R., Collins, D., Jonsson, H., Schmid, B. and Wang, J. (2006). Comparison of methods for deriving aerosol asymmetry parameter. *J. Geophys. Res*. 111: D05S04.

Artaxo, P., Fernandes, E.T., Martins, J.V., Yamasoe, M.A., Hobbs, P.V., Maenhaut, W., Longo, K.M. and Castanho, A. (1998). Large scale aerosol source apportionment in Amazonia. *J. Geophys. Res.* 103: 31837–31848.

Artaxo, P. (2001). The Atmospheric Component of Biogeochemical Cycles in the Amazon Basin. In *The Biogeochemistry of the Amazon Basin*, McClain, M.E., Victoria, R.L., Richey, J.E. (Eds.), Oxford University Press, pp. 42–52.

Artaxo, P., Martins, J.V., Yamasoe, M.A., Proc´opio, A.S., Pauliquevis, T.M., Andreae, M.O., Guyon, P., Gatti, L.V. and Leal, A.M.C. (2002). Physical and chemical properties of aerosols in the wet and dry seasons in Rondônia, Amazonia. *J. Geophys. Res*. 107: 8081.

Campbell, J.R., Reid, J.S., Westphal, D.L., Zhang, J., Tackett, J.L., Chew, B.N., Welton, E.J., Shimizu, A., Sugimoto, N., Aoki, K. and Winker, D.M. (2013). Characterizing the vertical profile of aerosol particle extinction and linear depolarization over Southeast Asia and the Maritime Continent: The 2007–2009 view from CALIOP. *Atmos. Res*. 122: 520–543.

Carmichael, G.R., Ferm, M., Thongboonchoo, N., Woo, J.H., Chan, L.Y., Murano, K., Viet, P.H., Mossberg, C., Bala, R., Boonjawat, J., Upatum, P., Mohan, M., Adhikary, S.P., Shrestha, A.B., Pienaar, J.J., Brunke, E.B., Chen, T., Jie, T., Guoan, D., Peng, L.C., Dhiharto, S., Harjanto, H., Jose, A.M., Kimani, W., Kirouane, A., Lacaux, J.P., Richard, S., Barturen, O., Carrasco Cerda, J., Athayde, A., Tavares, T., Cotrina, J.S. and Bilici, E. (2003). Measurements of sulfur dioxide, ozone and ammonia concentrations in Asia, Africa, and South America using passive samplers. *Atmos. Environ*. 37: 1293–1308.

Chuang, M.T., Chang, S.C., Lin, N.H., Wang, J.L., Sheu, G.R., Chang, Y.J. and Lee, C.T. (2013a). Aerosol chemical properties and related pollutants measured in Dongsha Island in the northern South China Sea during 7-SEAS/Dongsha Experiment. *Atmos. Environ*. 78: 82–92.

Chuang, M.T., Chou, C.C.K., Sopajaree, K., Lin, N.H., Wang, J.L., Sheu, G.R., Chang, Y.J. and Lee, C.T. (2013b). Characterization of aerosol chemical properties from near-source biomass burning in the northern Indochina during 7-SEAS/Dongsha experiment. *Atmos. Environ*. 78: 72–81.

Chuang, M.T., Fu, J.S., Lee, C.T., Lin, N.H., Gao, Y., Wang, S.H., Sheu, G.R., Hsiao, T.C., Wang, J.L., Yen, M.C., Lin, T.H. and Thongboonchoo, N. (2016). The simulation of long-range transport of biomass burning plume and short-range transport of anthropogenic pollutants to a mountain observatory in East Asia during the 7-SEAS/2010 Dongsha Experiment. *Aerosol Air Qual. Res*. 16: 2933–2949.

Crutzen, P.J. and Andreae, M.O. (1990). Biomass burning in the tropics: Impact on atmospheric chemistry and biogeochemical cycles. *Science* 250: 1669–1678.

Draxler, R.R. and Rolph, G.D. (2003). HYSPLIT (HYbrid Single-Particle Lagrangian Integrated Trajectory) Model Access via NOAA ARL READY Website. NOAA Air Resources Laboratory, Silver Spring, MD. http://www.arl.noaa.gov/ready/hysplit4.html.

Dubovik, O., Holben, B.N., King, M.D., Tanré, D. and Slutsker, I. (2002). Variability of absorption and optical properties of key aerosol types observed in world wide locations. *J. Atmos. Sci*. 59: 590–608.

Dubovik, O., Sinyuk, A., Lapyonok, T., Holben, B.N., Mishchenko, M., Yang, P., Eck, T.F., Volten, H., Muñoz, O., Veihelmann, B., van der Zande, W.J., Leon, J.F., Sorokin, M. and Slutsker, I. (2006). Application of spheroid models to account for aerosol particle nonsphericity in remote sensing of desert dust. *J. Geophys. Res*. 111: D11208.

Eck, T.F., Holben, B.N., Reid, J.S., Dubovik, O., Smirnov, A., O'Neill, N.T., Slutsker, I. and Kinne, S. (1999). Wavelength dependence of the optical depth of biomass burning, urban, and desert dust aerosols. *J. Geophys. Res*. 104: 31333–31349.

Eck, T.F., Holben, B.N., Ward, D.E., Mukelabai, M.M., Dubovik, O., Smirnov, A., Schafer, J.S., Hsu, N.C., Piketh, S.J., Queface, A., Le Roux, J., Swap, R.J. and Slutsker, I. (2003). Variability of biomass burning aerosol optical characteristics in southern Africa during the SAFARI 2000 dry season campaign and a comparison of single scattering albedo estimates from radiometric measurements. *J. Geophys. Res*. 108: 8477.

Forster, P., Ramaswamy, V., Artaxo, P., Berntsen, T., Betts, R.A., Fahey, D.W., Haywood, J., Lean, J., Lowe, D.C., Myhre, G., Nganga, J., Prinn, R., Raga, G., Schulz, M. and Van Dorland, R. (2007). Changes in Atmospheric Constituents and Radiative Forcing. Chapter 2 of the *Climate Change 2007: The Physical Science Basis*, IPCC – Intergovernmental Panel on Climate Change Book. Cambridge University Press, United Kingdom, ISSN 978-0-521-88009-1.

Fu, J.S., Hsu, N.C., Gao, Y., Huang, K., Li, C., Lin, N.H. and Tsay, S.C. (2012). Evaluating the influences of biomass burning during 2006 BASE-ASIA: A regional chemical transport modeling. *Atmos. Chem. Phys*. 12: 3837–3855.

Gautam, R., Hsu, N.C., Eck, T.F., Holben, B.N., Janjai, S., Jantarach, T., Tsay, S.C. and Lau, W.K. (2013). Characterization of aerosols over the Indochina peninsula from satellite-surface observations during biomass burning pre-monsoon season. *Atmos. Environ*. 78: 51–59.

Haywood, J.M. and Boucher, O. (2000). Estimates of the direct and indirect radiative forcing due to tropspheric aerosols: A review. *Rev. Geophys*. 38: 513–543.

Haywood, J.M., Osborne, S.R., Francis, P., Keil, A., Formenti, P., Andrea, M. and Kaye, P. (2003). The mean physical and optical properties of regional haze dominated by biomass burning aerosol measured from the C-130 aircraft during SAFARI 2000. *J. Geophys. Res*. 108: 8473.

Hess, M., Koepke, P. and Schult, I. (1998). Optical properties of aerosols and clouds: The software package OPAC. *Bull. Am. Meteorol. Soc*. 79: 831–44.

Hobbs, P.V., Reid, J.S., Kotchenruther, R.A., Ferek, R.J. and Weiss, R. (1997). Direct radiative forcing by smoke from biomass burning. *Science* 275: 1776–1778.

Hobbs, P.V., Sinha, P., Yokelson, R.J., Christian, T.J., Blake, D.R., Gao, S., Kirchstetter, T.W., Novakov, T. and Pilewskie, P. (2003). Evolution of gases and particles from a savanna fire in South Africa. *J. Geophys. Res*. 108: 8485.

Holben, B.N., Eck, T.F., Slutsker, I., Smirnov, A., Sinyuk, A., Schafer, J., Giles, D. and Dubovik, O. (2006). Aeronet's Version 2.0 quality assurance criteria. *Proc. SPIE* 6408: 64080Q.

Hsiao, T.C., Ye, W.C., Wang, S.H., Tsay, S.C., Chen, W.N., Lin, N.H., Lee, C.T., Hung, H.M., Chuang, M.T. and Chantara, S. (2016). Investigation of the CCN activity, BC and UVBC mass concentrations of biomass burning aerosols during the 2013 BASELInE campaign. *Aerosol Air Qual. Res.* 16: 2742–2756.

Huang, J., Hsu, N.C., Tsay, S.C., Jeong, M.J., Holben, B.N., Berkoff, T.A. and Welton, E.J. (2011). Susceptibility of aerosol optical thickness retrievals to thin cirrus contamination during the BASE-ASIA campaign. *J. Geophys. Res.* 116: D08214.

Huang, K., Fu, J.S., Hsu, N.C., Gao, Y., Dong, X., Tsay, S.C. and Lam, Y.F. (2013). Impact assessment of biomass burning on air quality in Southeast and East Asia during BASE-ASIA. *Atmos. Environ.* 78: 291–302.

IPCC (2001). Climate Change 2001: The Scientific Basis—Contribution of Working Group I to the Third Assessment Report of the Intergovernmental Panel on Climate Change, Houghton J.T. *et al*., (Eds.), Cambridge Univ. Press, New York.

IPCC (2007). Climate Change 2007: Contribution of Working Group III to the Fourth Assessment Report of the Intergovernmental Panel on Climate Change, Metz, B.,

Davidson, O.R., Bosch, P.R., Dave, R. and Meyer, L.A. (Eds.), Cambridge University Press, Cambridge, United Kingdom and New York, NY, USA.

IPCC (2014). IPCC Fifth Assessment Report, Climate Change 2013: The Physical Science Basis. https://www.ipcc.ch/report/ar5/wg1/, Last Access: April 2, 2014.

Jacob, D.J., Crawford, J.H., Kleb, M.M., Connors, V.S., Bendura, R.J., Raper, J.L., Sachse, G.W., Gille, J.C., Emmons, L. and Heald, C.L. (2003). Transport and Chemical Evolution over the Pacific (TRACE-P) aircraft mission: Design, execution, and first results. *J. Geophys. Res*. 108: 9000.

Jacobson, M.Z. (2000). A physically-based treatment of elemental carbon optics: Implications for global direct forcing of aerosols. *Geophys. Res. Lett*. 27: 217–220.

Janjai, S., Suntaropas, S. and Nunez, M. (2009). Investigation of aerosol optical properties in Bangkok and suburbs. *Theor. Appl. Climatol.* 96: 221–233.

Johnson, B.T., Osborne, S.R., Haywood, J.M. and Harrison, M.A.J. (2008). Aircraft measurements of biomass burning aerosol over West Africa during DABEX. *J. Geophys. Res*. 113: D00C06.

Kaufman, Y.J., Tanré, D. and Boucher, O. (2002). A satellite view of aerosols in the climate system. *Nature* 419: 215–223.

Khamkaew, C., Chantara, S., Janta, R., Pani, S.K., Prapamontol, T., Kawichai, S., Wiriya, W. and Lin, N.H. (2016). Investigation of biomass burning chemical components over Northern Southeast Asia during 7-SEAS/BASELInE 2014 campaign. *Aerosol Air Qual. Res.* 16: 2655–2670.

Koepke, P., Hess, M., Schult, I. and Shettle, E.P. (1997). Global Aerosol Data Set. Report No. 243, Max-Planck-Institut für Meteorologie, Hamburg.

Lee, C.T., Ram, S.S., Nguyen, D.L., Chou, C.C.K., Chang, S.Y., Lin, N.H., Chang, S.C., Hsiao, T.C., Sheu, G.R., Ou-Yang, C.F., Chi, K.H., Wang, S.H. and Wu, X.C. (2016a). Aerosol chemical profile of near-source biomass burning smoke in Sonla, Vietnam during 7-SEAS campaigns in 2012 and 2013. *Aerosol Air Qual. Res.* 16: 2603–2617.

Lee, J., Hsu, N.C., Bettenhausen, C., Sayer, A.M., Seftor, C.J., Jeong, M.J., Tsay, S.C., Welton, E.J., Wang, S.H. and Chen, W.N. (2016b). Evaluating the height of biomass burning smoke aerosols retrieved from synergistic use of multiple satellite sensors over Southeast Asia. *Aerosol Air Qual. Res.* 16: 2831–2842.

Li, Z. and Kou, L. (1998). Atmospheric direct radiative forcing by smoke aerosols determined from satellite and surface measurements. *Tellus Ser. B* 50: 543–554.

Lin, N.H., Tsay, S.C., Reid, J.S., Yen, M.C., Sheu, G.R., Wang, S.H., Chi, K.H., Chuang, M.T., Ou-Yang, C.F., Fu, J.S., Lee, C.T.,Wang, L.C., Wang, J.L., Hsu, C.N., Holben, B.N., Chu, Y.C., Maring, H.B., Nguyen, A.X., Sopajaree, K., Chen, S.J., Cheng, M.T., Tsuang, B.J., Tsai, C.J., Peng, C.M., Chang, C.T., Lin, K.S., Tsai, Y.I., Lee, W.J., Chang, S.C., Liu, J.J. and Chiang, W.L. (2013). An overview of regional experiments on biomass burning aerosols and related pollutants in Southeast Asia: From BASE-ASIA and the Dongsha Experiment to 7-SEAS. *Atmos. Environ.* 78: 1–19.

Lin, N.H., Sayer, A.M., Wang, S.H., Loftus, A.M., Hsiao, T.C., Sheu, G.R., Hsu, N.C., Tsay, S.C. and Chantara, S. (2014). Interactions between biomass-burning aerosols and clouds over Southeast Asia: Current status, challenges, and perspectives. *Environ. Pollut*. 195: 292–307.

Liou, K.N. (1980). *An Introduction to Atmospheric Radiation*. Academic Press, San Diego, Calif, pp. 392.

Loftus, A.M., Tsay, S.C., Pantina, P., Nguyen, C., Gabriel, P.M., Nguyen, X.A., Sayer, A.M., Tao, W.K. and Matsui, T. (2016). Coupled aerosol-cloud systems over Northern Vietnam during 7-SEAS/BASELInE: A radar and modeling perspective. *Aerosol Air Qual. Res.* 16: 2768–2785.

Manual of Remote Sensing (1975). American Society of Photogrammetry, Reeves, R.G. Anson, A. and Landen, D. (Eds.), 1st Ed., Falls Church, Va.

McClatchey, R.A., Fenn, R.W., Selby, J.E.A., Volz, F.E. and Garing, J.S. (1972). Optical Properties of the Atmosphere, (third edition), Air Force Cambridge Research Laboratories, Report AFCRL-72-0497.

Michalsky, J., Anderson, G.P., Barnard, J., Delamere, J., Gueymard, C., Kato, S., Kiedron, P., McComiskey, A. and Ricchiazzi, P. (2006). Shortwave radiative closure studies for clear skies during the atmospheric radiation measurement 2003 aerosol intensive observation period. *J. Geophys. Res*. 111: D14S90.

Miller, J. and O'Neill, T. (1997). Multilatitude airborne observations of insolation effects of forest fire smoke aerosols at BOREAS: Estimates of aerosol optical properties. *J. Geophys. Res.* 102: 29729–29736.

Moody, E.G., King, M.D., Platnick, S., Schaaf, C.B. and Gao, F. (2005). Spatially complete global spectral surface albedos: Value-added datasets derived from TERRA MODIS land products. *IEEE Trans. Geosci. Remote Sens.* 43: 144–158.

Myhre, G., Berntsen, T.K., Haywood, J.M., Sundet, J.K., Holben, B.N., Johnsrud, M. and F. Stordal (2003). Modeling the solar radiative impact of aerosols from biomass burning during the Southern African Regional science initiative (SAFARI-2000) experiment. *J. Geophys. Res.* 108: 8501.

Pani, S.K. (2013). *Sources and Radiative Effects of Ambient Aerosols in an Urban Atmosphere in East India*. Ph. D. Thesis. Indian Institute of Technology Kharagpur, India.

Pani, S.K. and Verma, S. (2014). Variability of winter and summertime aerosols over Eastern India urban environment. *Atmos. Res*. 137: 112–124.

Pani, S.K., Wang, S.H., Lin, N.H., Tsay, S.C., Lolli, S., Chuang, M.T., Lee, C.T., Chantara, S. and Yu, J.Y. (2016a). Assessment of aerosol optical property and radiative effect for the layer decoupling cases over the Northern South China Sea during the 7-SEAS/Dongsha Experiment. *J. Geophys. Res*. 121: 4894–4906.

Pani, S.K., Wang, S.H., Lin, N.H., Lee, C.T., Tsay, S.C., Holben, B.N., Janjai, S., Hsiao, T.C., Chuang, M.T. and Chantara, S. (2016b). Impact of Springtime Biomass-Burning Aerosols on Radiative Forcing over Northern

Thailand during the 7-SEAS Campaign. EGU General Assembly 2016, 17–22 April, 2016, Vienna Austria, p. 11795.

Pantina, P., Tsay, S.C., Hsiao, T.C., Loftus, A.M., Kuo, F., Ou-Yang, C.F., Sayer, A.M., Wang, S.H., Lin, N.H., Hsu, N.C., Janjai, S., Chantara, S. and Nguyen, A.X. (2016). COMMIT in 7-SEAS/BASELInE: Operation of and observations from a novel, mobile laboratory for measuring in-situ properties of aerosols and gases. *Aerosol Air Qual. Res.* 16: 2728–2741.

Patadia, F., Gupta, P., Christopher, S.A. and Reid, J.S. (2008). A multisensor satellite-based assessment of biomass burning aerosol radiative impact over Amazonia. *J. Geophys. Res*. 113: D12214.

Penner, J.E., Dickinson, R.E. and O'Neill, C.A. (1992). Effects of aerosol from biomass burning on the global radiation budget. *Science* 256: 1432–1434.

Petzold, A., Kopp, C. and Neissner, R. (1997). The dependence of the specific attenuation cross-section on the black carbon mass fraction and particle size. *Atmos. Environ*. 31: 661–672.

Procopio, A., Artaxo, P., Kaufman, Y., Remer, L., Schafer, J. and Holben, B. (2004). Multiyear analysis of Amazonian biomass burning smoke radiative forcing of climate. *Geophys. Res. Lett*. 31: 3108–3112.

Ramachandran, S., Srivastava, R., Kedia, S. and Rajesh, T.A. (2012). Contribution of natural and anthropogenic aerosols to optical properties and radiative effects over an urban location. *Environ. Res. Lett*. 7: 034028.

Ramanathan, V., Crutzen, P.J., Kiehl, J.T. and Rosenfeld, D. (2001). Aerosols, climate and the hydrological cycle. *Science* 294: 2119–2124.

Reid, J.S. and Hobbs, P.V. (1998). Physical and optical properties of young smoke from individual biomass fires in Brazil. *J. Geophys. Res*. 103: 32013–32030.

Reid, J.S., Hyer, E.J., Johnson, R.S., Holben, B.N., Yokelson, R.J., Zhang, J., Campbell, J.R., Christopher, S.A., Di Girolamo, L., Giglio, L., Holz, R.E., Kearney, C., Miettinen, J., Reid, E.A., Turk, F.J., Wang, J., Xian, P., Zhao, G., Balasubramanian, R., Chew, B.N., Janjai, S., Lagrosas, N., Lestari, P., Lin, N.H., Mahmud, M., Nguyen, A.X., Norris, B., Oanh, N.T.K., Oo, M., Salinas, S.V., Welton, E.J. and Liew, S.C. (2013). Observing and understanding the Southeast Asian aerosol system by remote sensing: An initial review and analysis for the Seven Southeast Asian Studies (7SEAS) program. *Atmos. Res*. 122: 403–468.

Ricchiazzi, P., Yang, S., Gautier, C. and Sowle, D. (1998). SBDART: A research and teaching tool for plane-parallel radiative transfer in the earth's atmosphere. *Bull. Am. Meteorol. Soc*. 79: 2101–2114.

Ross, J., Hobbs, P. and Holben B. (1998). Radiative characteristics of regional hazes dominated by smoke from biomass burning in Brazil: Closure tests and direct radiative forcing. *J. Geophys. Res*. 103: 31925–31941.

Satheesh, S.K. and Ramanathan, V. (2000). Large differences in tropical aerosol forcing at the top of the atmosphere and earth's surface. *Nature.* 405: 60–63.

Satheesh, S.K. (2002). Radiative forcing by aerosols over Bay of Bengal region. *Geophys. Res. Lett*. 29: 2083.

Satheesh, S.K., Vinoj, V., and Moorthy, K.K. (2010). Radiative effects of aerosols at an urban location in Southern India: Observations versus model. *Atmos. Environ*. 44: 5295–5304.

Sayer, A.M., Hsu, N.C., Eck, T.F., Smirnov, A. and Holben, B.N. (2013). AERONET-based models of smoke-dominated aerosol near source regions and transported over oceans, and implications for satellite retrievals of aerosol optical depth. *Atmos. Chem. Phys*. 14: 11493–11523.

Sayer, A.M., Hsu, N.C., Hsiao, T.C., Pantina, P., Kuo, F., Ou-Yang, C.F., Holben, B.N., Janjai, S., Chantara, S., Wang, S.H., Loftus, A.M., Lin, N.H. and Tsay, S.C. (2016). In-situ and remotely-sensed observations of biomass burning aerosols at Doi Ang Khang, Thailand during 7-SEAS/BASELInE 2015. *Aerosol Air Qual. Res.* 16: 2786–2801.

Sena, E.T., Artaxo, P. and Correia, A.L. (2013). Spatial variability of the direct radiative forcing of biomass burning aerosols and the effects of land use change in Amazonia. *Atmos. Chem. Phys*. 13: 1261–1275.

Smirnov, A., Holben, B.N., Eck, T.F., Dubovik, O. and Slutsker, I. (2000). Cloud-screening and quality control algorithms for the AERONET database. *Remote Sens. Environ*. 73: 337–349.

Srivastava, R. and Ramachandran, S. (2013). The mixing state of aerosols over the indo-gangetic plain and its impact on radiative forcing. *Q. J. R. Meteorolog. Soc.* 139: 137–151.

Stamnes, K., Tsay, S.C., Wiscombe, W. and Jayaweera, K. (1988). Numerically stable algirithm for discrete-ordinate-method radiative transfer in multiple scattering and emitting layered media. *Appl. Opt.* 27: 2502–2509.

Streets, D.G., Yan, F., Chin, M., Diehl, T., Mahowald, N., Schultz, M., Wild, M., Wu, Y. and Yu, C. (2009). Anthropogenic and natural contributions to regional trends in aerosol optical depth. *J. Geophys. Res*. 114: 1980–2006.

Tsay, S.C., Hsu, N.C., Lau, W.K.M., Li, C., Gabriel, P.M., Ji, Q., Holben, B.N., Judd Welton, E., Nguyen, A.X., Janjai, S., Lin, N.H., Reid, J.S., Boonjawat, J., Howell, S.G., Huebert, B.J., Fu, J.S., Hansell, R.A., Sayer, A.M., Gautam, R., Wang, S.H., Goodloe, C.S., Miko, L.R., Shu, P.K., Loftus, A.M., Huang, J., Kim, J.Y., Jeong, M.J. and Pantina, P. (2013). From BASE-ASIA toward 7-SEAS: A satellite-surface perspective of boreal spring biomass-burning aerosols and clouds in Southeast Asia. *Atmos. Environ*. 78: 20–34.

Tsay, S.C., Maring, H.B., Lin, N.H., Buntoung, S., Chantara, S., Chuang, H.C., Gabriel, P.M., Goodloe, C.S., Holben, B.N., Hsiao, T.C., Hsu, N.C., Janjai, S., Lau, W.K.M., Lee, C.T., Lee, J., Loftus, A.M., Nguyen, A.X., Nguyen, C.M., Pani, S.K., Pantina, P., Sayer, A.M., Tao, W.K., Wang, S.H., Welton, E.J., Wiriya, W. and Yen, M.C. (2016). Satellite-surface perspectives of air quality and aerosol-cloud effects on the environment: An overview of 7-SEAS/BASELInE. *Aerosol Air Qual. Res.* 16: 2581–2602.

Twomey, S. (1977). The influence of pollution on the

shortwave albedo of clouds. *J. Atmos. Sci*. 34: 1149–1152.

Vakkari, V., Kerminen, V.M., Beukes, J.P., Tiitta, P., Zyl, P.G.V., Josipovic, M., Venter, A.D., Jaars, K., Worsnop, D.R., Kulmala, M. and Laakso, L. (2014). Rapid changes in biomass burning aerosols by atmospheric oxidation. *Geophys. Res. Lett*. 41: 2644–2651.

Verma, S., Pani, S.K. and Bhanja, S.N. (2013). Sources and radiative effects of wintertime black carbon aerosols in an urban atmosphere in East India. *Chemosphere* 90: 260–269.

Wang, S.H., Welton, E.J., Holben, B.N., Tsay, S.C., Lin, N.H., Giles, D., Stewart, S.A., Janjai, S., Nguyen, X.A., Hsiao, T.C., Chen, W.N., Lin, T.H., Buntoung, S., Chantara, S. and Wiriya, W. (2015). Vertical distribution and columnar optical properties of springtime biomass-burning aerosols over Northern Indochina during 2014 7-SEAS campaign. *Aerosol Air Qual. Res.* 15: 2037–2050.

Watson, J.G., Chow, J.C. and Chen, L.W.A. (2005). Summary of organic and elemental carbon/black carbon analysis methods and intercomparisons. *Aerosol Air Qual. Res*. 5: 65–102.

Received for review, March 29, 2016
Revised, August 5, 2016
Accepted, September 7, 2016